The International Journal of Advanced Manufacturing Technology (2019) 104:2887–2898
https://doi.org/10.1007/s00170-019-04195-y

ORIGINAL ARTICLE

Closed loop control of melt pool width in robotized laser powder–directed energy deposition process

Meysam Akbari[1] · Radovan Kovacevic[1]

Received: 8 March 2019 / Accepted: 23 July 2019 / Published online: 31 July 2019

Abstract
Robotized laser powder–directed energy deposition is a non-linear process, and the dynamic response of the system varies layer by layer. An adaptable PI controller with layer-dependent control gains was developed to ensure a constant melt pool width through the entire build. The laser power was selected as the control output variable, and the melt pool width was chosen as the control input variable. The performance of the controller was evaluated through deposition of thin wall samples. The results showed that the controller, by adjusting the laser power in real time, could successfully maintain the melt pool width and produce a more uniform and finer microstructure as compared to the sample with a constant laser power.

Keywords Robotized laser powder–directed energy deposition · Closed loop control system · Melt pool image monitoring · Microstructure and mechanical properties · Additive manufacturing

1 Introduction

Additive manufacturing (AM) is a technique used to fabricate parts in a layer-wise fashion. This technique offers reduction in time and material waste, leading to a decreased buy-to-fly ratio [1]. Different AM techniques that utilize metal as material supply have been researched in recent years. Powder bed fusion (PBF) and directed energy deposition (DED) are the two well-recognized sub-categories of metal AM processes [2]. DED is defined as "an additive manufacturing process in which focused thermal energy is used to fuse materials by melting as they are being deposited," according to ISO/ASTM 52900:2015 [3]. In the DED process, metallic powder, wire, or a combination of both is fed into the melt pool that is formed by a high energy focused heat source such as electron beam, arc, or laser. In contrast, powder bed fusion process works based on a bed of powder that is selectively sintered or melted via laser or electron beam heat source. Using PBF process, building of highly complex parts with internal features is possible. Surface finish of final buildup is also far better than DED process. However, PBF-processed parts are associated with different issues. Fotovvati et al. [4] showed the inconsistency and variation of microstructural and mechanical properties of AM Ti-6Al-4V sheets in different directions and thicknesses. There are numerous advantages of using DED with respect to the PBF process, including an unlimited buildup size, a higher deposition rate, and the possibility to make functionally graded compositions. DED can repair worn out or damaged high value components and decrease the need for the support structure. Utilization of sensors for the purpose of monitoring and control is also common in DED, helping the researchers to better understand the physics of the process. Laser powder–directed energy deposition or commonly known as LENS® (Laser Engineered Net Shaping) has been extensively used in literature for different applications. For instance, Hu and Kovacevic [5] used multiple powder feeding systems to print functionally graded structures to tailor the mechanical and compositional properties of the buildup. Wilson et al. [6] showed the effectiveness of the laser powder feeding process to repair and remanufacture a damaged turbine blade. Yaoyu et al. [7] employed a robotized laser-based powder feeding system to print metamaterials with exotic behavior such as negative coefficient of thermal expansion or large Poisson's ratio. Beside the tremendous advantages of laser DED process,

✉ Radovan Kovacevic
kovacevi@lyle.smu.edu

[1] Research Center for Advanced Manufacturing, Southern Methodist University, 3101 Dyer Street, Dallas, TX 75205, USA

one main concern is the energy efficiency of this process. Lin et al. [8] established an empirical model to characterize a relationship between process parameters and energy efficiency, and they were able to improve the energy efficiency of DED process significantly.

In robotized laser powder–directed energy deposition (RLP-DED), the main processing variables such as powder flow rate, laser power, layer thickness, travel speed, and step-over value affect the quality of deposition and stability of the process. Optimization and tuning of these parameters are necessary prior to the process in order to achieve a consistent and stable process. However, due to the existence of disturbances such as change in the thermal condition (usually heat transfer mode changes from 3D to 2D conduction during the process) or small change in variables like thermal conductivity (a temperature-dependent material property), powder flow rate, or laser power, the implementation of an in situ sensing and control system is required.

Bi et al. [9] used IR temperature signals from a single-wall deposition in order to develop a feedback system in the laser powder feeding process. They tried to maintain the melt pool temperature as a control input by adjusting the laser power as a control variable. Their result showed a nearly constant melt pool size and homogeneous microstructure. Farshidianfar et al. [10] developed a feedback proportional integral derivative (PID) controller based on an infrared imaging system in the laser powder cladding process. They were able to maintain the cooling rate by adjusting the travel speed. They showed that the closed loop controller was capable of producing a relatively consistent microstructure. Yaoyu et al. [11] developed a sensing and control system in a robotized laser powder deposition system. They utilized an infrared imaging system to monitor the melt pool size in real time and adjusted the laser power as the control output. They verified the performance of the controller by achieving a uniform cross-sectional thickness of the L-shaped component. Hofman et al. [12] employed a CMOS camera to obtain the width of the melt pool in the laser powder cladding process. They showed that constant laser power can produce higher degrees of dilution and lower value of microhardness in the cladded layer. However, after applying a feedback system, the laser power was reduced by 50%, and hardness and dilution of the clads remained constant. Heralic et al. [13] proposed a controller for the laser wire direct metal deposition system. Their controller was composed of a PI controller, to maintain the melt pool width, and a feedforward compensator, to keep the layer height consistent. The controller was able to increase the stability by minimizing the risk of droplet formation and stubbing.

Most of the studies related to closed loop control of laser-directed energy deposition have relied on fixed parameters of the control algorithm. These researches have mainly dealt with a cladding process or a part with a few layers of deposition, where the disturbances such as change in the heat transfer mode or cooling rate had a relatively low effect on the dynamics of the process. Therefore, the control parameters were considered to be fixed values during the process. The existence of disturbances could make the process highly non-linear. For instance, the relation between the melt pool size or temperature and laser power is typically non-linear throughout the entire process, especially when the structure has numerous layers.

In this paper, a monitoring and a PI-closed loop controller based on an infrared imaging system were set up on a robotized laser powder–directed energy deposition system. The aim of the work was to investigate the different responses of the non-linear laser deposition process and present a more accurate and reliable controller. The performance of the controller was evaluated by deposition of a 160-layer stainless steel 316L thin wall part. The resulting microstructure was discussed and compared with a deposition under constant laser power.

2 Experimental procedure

The block diagram of the RLP-DED system is shown in Fig. 1. The system included a 6-axis KUKA robotic arm (KR60) coupled with a two axis positioning table, an IPG 4-kW fiber laser with wavelength of 1070 nm, a laser welding head (Precitec YW50), and an in-house powder feeder [14]. The laser spot was 2 mm in diameter which was achieved at 17 mm defocused distance below the focal point. The image monitoring system was based on a CMOS camera (Prosilica GC 640) that was coaxially mounted on the laser head. The camera worked on a monochrome mode with a resolution of 640 × 480 pixels, corresponding to a maximum acquisition of 200 frames per second.

The thin wall samples were fabricated by using the optimized process parameters listed in Table 1. All parameters except laser power were kept constant during the process for both samples with constant and controlled laser power.

The depositions were carried out using austenitic Stainless Steel 316L powder produced by North American Hoganas High Alloys LLC. The powder with a particle size of 50–150 μm was deposited onto the SS 304L plates as substrate. Chemical composition of the powder and substrate are listed in Table 2.

Both samples, i.e., the sample with constant laser power and the sample with controlled laser power, were cross cut and mounted for metallurgical analysis. Then, the samples were sanded and a diamond polishing pad was used to polish them. Afterward, they were chemically etched in HCL:HNO_3 = 3:1 solution for 45 s. A scanning electron microscope (SEM LEO 1450) and an optical microscope (Olympus DP72) were used for microstructural analysis.

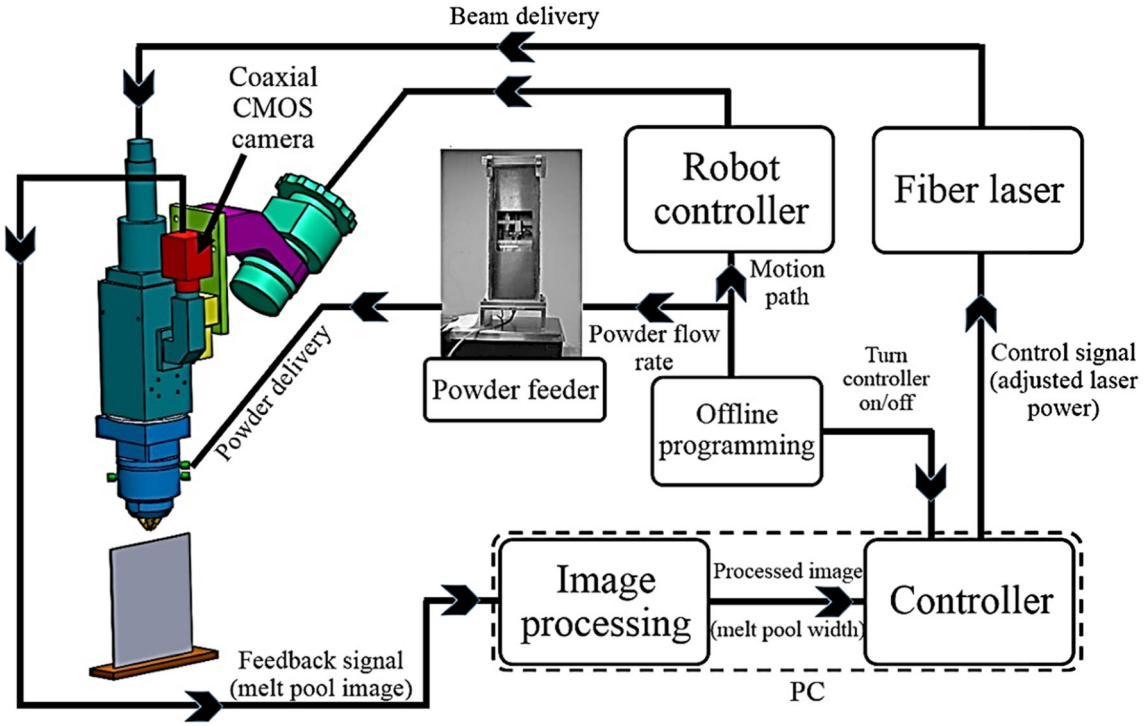

Fig. 1 Schematic overview of robotized laser powder–directed energy deposition equipped with closed loop control system

3 Closed loop control system

3.1 Image acquisition and processing

The melt pool width, as the process variable or control variable, was monitored and controlled in real time. The CMOS camera was coaxially mounted on the laser head to take the melt pool images from the top view. All the lights from the melt pool including laser radiation and heat radiation were reflected by a dichroic mirror placed inside the laser head and received by a camera chip. A long-pass infrared filter was utilized in front of the camera to pass the light with a wavelength greater than 700 nm. A notch filter that blocks the laser light with a wavelength of 1070 nm was also used in order to protect the camera from laser damage.

A typical acquired image of the melt pool by a camera equipped with infrared filter is shown in Fig. 2(a). Figure 2 shows the steps taken to process the raw image from the camera to eventually measure the width of the melt pool. The image processing code was developed by using the Vision Acquisition Module of Labview platform and was implemented in real time. In the first step, a gray level (0–255) image is captured by the camera (Fig. 2(a)). Then, the image is converted to a binary, black-and-white image by applying a user-defined threshold value (Fig. 2(b)). The threshold was obtained by depositing several tracks with different widths. Then, the measurement of track widths was taken and compared with the corresponding images to get the appropriate threshold value. The value of the threshold was chosen to be 80 in the experiments. As is seen from Fig. 2(b), the melt pool is surrounded by some flare that is produced by the hot powder particles. The flare can cause considerable noise and error in measuring the melt pool width. Therefore, a low-pass FFT (Fast Fourier Transform) filter was employed. The FFT of an image represents the frequencies of occurrence of pixel intensity variations in the original image (Fig. 2(c)). The consistent and smooth intensity variations in the image correspond to low frequencies in the FFT, while the abrupt and fast intensity variations in the image such as flare or noisy pixels at the edge of melt pool correspond to high frequencies in FFT. A low-

Table 1 Process parameters used in this study

Process parameters	Travel speed (mm/s)	Laser power (W)	Powder feed rate (g/s)	z-increment (mm)	Carrier gas* (l/min)	Shielding gas* (l/min)
Sample with constant laser power	5	600	0.4	0.5	8	15
Sample with controlled laser power	5	Adjustable by controller	0.4	0.5	8	15

*Argon was used as carrier and shielding gas

Table 2 Chemical composition of powder and substrate

Element (wt%)	C	Mn	Si	Ni	Mo	Cr	P	S	Fe
Powder (316L)	0.03	1.5	0.8	12	2.50	17	–	–	Bal.
Substrate (304L)	0.03	2	–	8	–	18	0.045	0.03	Bal.

pass filter with a cutoff frequency of 5% is utilized to remove the noise, while preserving the melt pool boundary as shown in Fig. 2(d). Frequency of each pixel is set to 0 if it is higher than cutoff frequency and remained unchanged if it is less than cutoff frequency. In the next step, the outline of melt pool is extracted (Fig. 2(e)). Ultimately, in order to measure the widest section of melt pool, all possible circles that were contained inside the outline were detected (Fig. 2(f)). The diameter of the largest circle was recognized as the melt pool width. Therefore, the melt pool width as the control variable was obtainable in real time.

3.2 System identification

The specific energy in the laser powder–directed energy deposition process is defined as the energy delivered to the process by the laser [15]:

$$E = \frac{P}{D \times \mathrm{TS}} \tag{1}$$

where P is the laser power, D is the laser beam diameter, and TS is the travel speed. The specific energy has a key role in determining the melt pool size, melt pool temperature, and morphology of the microstructure. However, given the fixed specific energy, it does not always guarantee a consistent melt pool size, temperature, or homogeneous microstructure. The existence of low frequent disturbances such as change in the heat transfer mode and change in material properties (e.g., thermal conductivity) requires that the specific energy be adjusted to ensure the stability of the process and quality of the deposition. In this study, the laser power that had a direct effect on specific energy was selected as an adjustable variable (control output). Melt pool width was chosen to be the control input.

To achieve a robust control system, it was essential to accurately identify and develop the dynamic model of the process. Experiments on the wall sample have shown that the dynamic relation between melt pool width and laser power is non-linear, especially in the initial layers. Therefore, a set of 10 step response tests were performed in the first 10 layers of a 160-layer thin wall part. The results of the tests are shown in Fig. 3.

There is no data available for the first layer in Fig. 3. This is because the process was unstable in the first layer, due to the extreme heat sink and large fluctuations in measurements; therefore, the step tests failed in this layer. In all step tests, the system was perturbed by increasing laser power abruptly from 500 to 600 W. This increase caused a change in the melt pool width. As can be seen in all layers, there was no overshoot in the responses. Therefore, the dynamic model of the process can be approximated by a first order with a time delay transfer function as [16]:

$$G(s) = \frac{K}{1 + \tau s} e^{-t_d s} \tag{2}$$

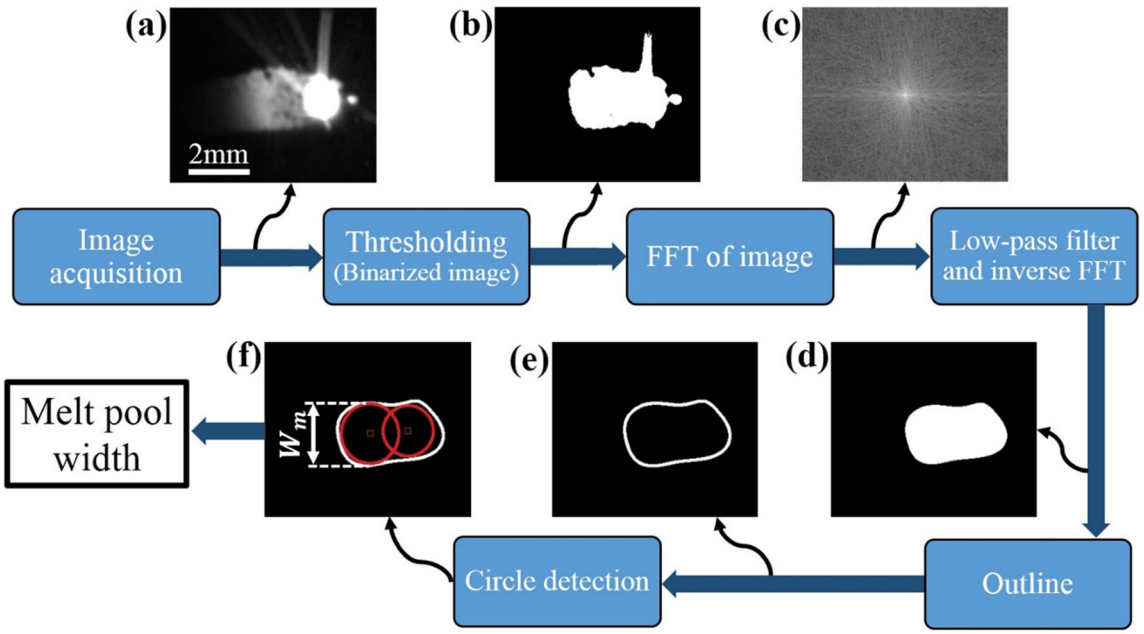

Fig. 2 Image processing steps to obtain the melt pool width (see text for details)

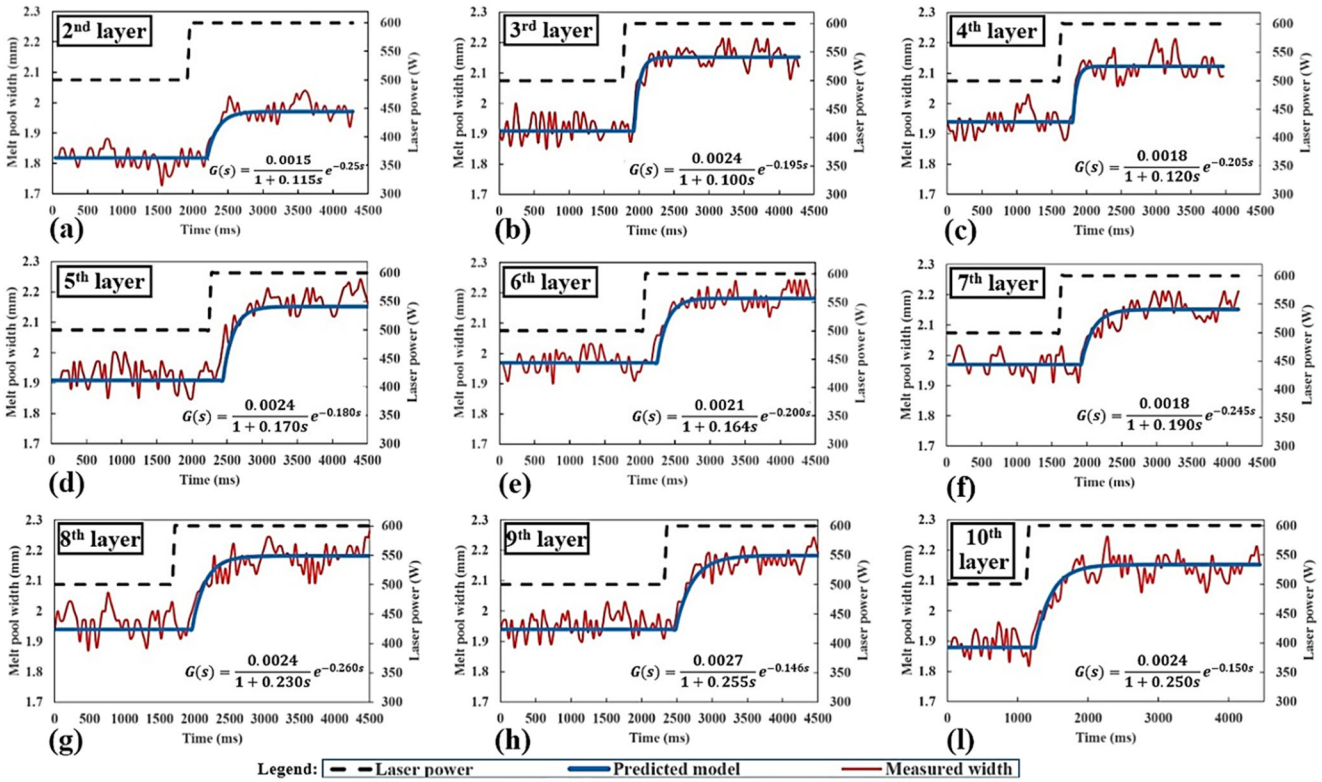

Fig. 3 The results of step response tests in different layers of a thin wall deposition. The corresponding transfer function of each layer 2 is displayed in the plots

where K is the static gain, τ is the time constant, and t_d is the time delay constant. The static gain is specified as the ratio between variations in the melt pool width (as output signal) and variations in the laser power (as input signal) after the steady state is reached ($K = \frac{\Delta W}{\Delta P}$). The time constant is the time that the response is required to reach 63% of its total change. The time delay or dead time is defined as the time interval where there is no change in the response after the step input is applied. These parameters are graphically illustrated in Fig. 4.

Experiments in the deposition of thin wall structure showed that the response of the system was almost the same inside each layer. However, from layer to layer, a new dynamic response was observed. This is mainly attributed to the change in thermal condition of the sample after a new layer was deposited. These changes were obvious from the 2nd layer up to the 8th layer, where the transfer function parameters, especially τ, indicated considerable variations. After the 9th layer, there was no change in parameters or their changes did not have effect on control parameters. This result will be discussed in detail in the next section. The step response tests were performed around the operating points in which the process was stable. The fluctuations in the melt pool width signal, which are seen in Fig. 3, were inherently associated with the laser-directed energy deposition process. The fluctuation amplitude could be attenuated by applying a digital smoothing filter. However, the filter could cause a delay in the response of the system. Therefore, use of a digital filter was avoided. The sampling frequency of the process was 30 Hz. This frequency was high enough to control the RLP-DED process with 5 mm/s travel speed.

The raw data from the step response tests was imported into the Pitops software from PiControl Solution LLC to identify the transfer functions of different layers. The corresponding predicted curves of the first-order time-delay transfer functions are depicted in the plots of Fig. 3. Also, the mathematical representation of the transfer functions is indicated in the plots.

3.3 Controller design

The block diagram of the closed loop control system is shown in Fig. 5. The melt pool width, as the user-defined set point (W_{SP}), was compared with the measured melt pool width (W_m). The W_m was obtained after the low-pass filter was applied on the raw image from the camera. The resulting error, $e(t) = W_{SP} - W_m$, was sent to the PID controller that was implemented in the Labview platform.

The PID controller has been extensively utilized in most industrial control applications due to its simple structure, high stability, and effectiveness. The PID controller is used when the mathematical model of the process is not available because of the complexity and non-linearity of the system. The output of the controller, i.e., laser power, was sent to the laser power

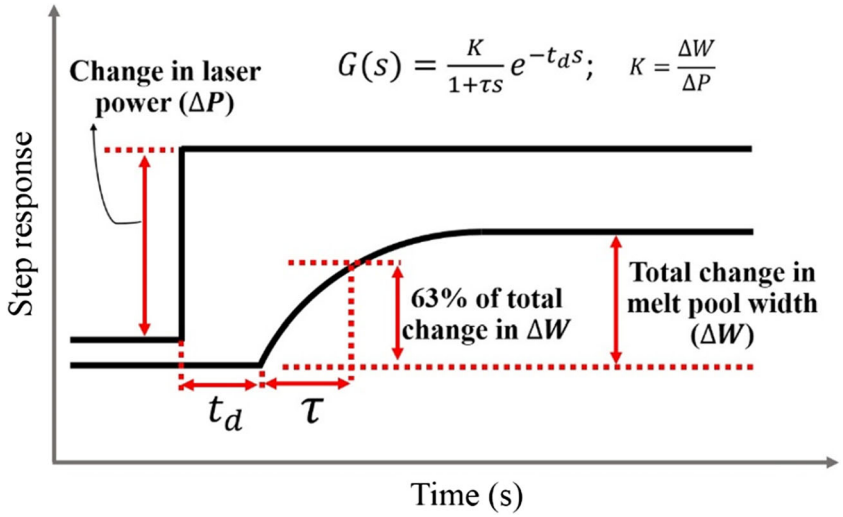

Fig. 4 Schematic illustration of parameters for first-order transfer function

unit. The time continuous equation used for the controller is as follows:

$$u(t) = K_c\left[e(t) + \frac{1}{T_i}\int_0^t e(\tau)d\tau + T_d\frac{de(t)}{dt}\right] \quad (3)$$

where $u(t)$ is the controller output sent to the laser unit as a voltage signal, K_c is the proportional gain, T_i is the integral gain, and T_d is the derivative gain. In order to digitally implement the time continuous equation in the computer, a finite difference approximation was used:

$$\int_0^t e(\tau)d\tau \approx \sum_{k=1}^{n} T_s e(kT_s) \quad (4)$$

$$\frac{de(t)}{dt} \approx \frac{e(nT_s) - e(nT_s - T_s)}{T_s} \quad (5)$$

where T_s is the sampling time, which was 0.033 s in this paper; n is the number of discretized steps between zero and time t; and k is the step number. Therefore, Eq. (3) is discretized as

$$u_n = K_c\left[e_n + \frac{1}{T_i}\sum_{k=1}^{n} T_s e_k + T_d\frac{e_n - e_{n-1}}{T_s}\right] \quad (6)$$

The tuning of PID gains was performed with Pitops software. Although, the derivative term could lead to faster response of the system, it caused oscillation and eventual instability in the system. Therefore, a PI algorithm was chosen to control the RLP-DED process in this work, and the derivative term was set at 0. As discussed in the previous section, the transfer function models of the first 10 layers were obtained through step response tests. Accordingly, the corresponding controller gains were achieved as is seen in Table 3.

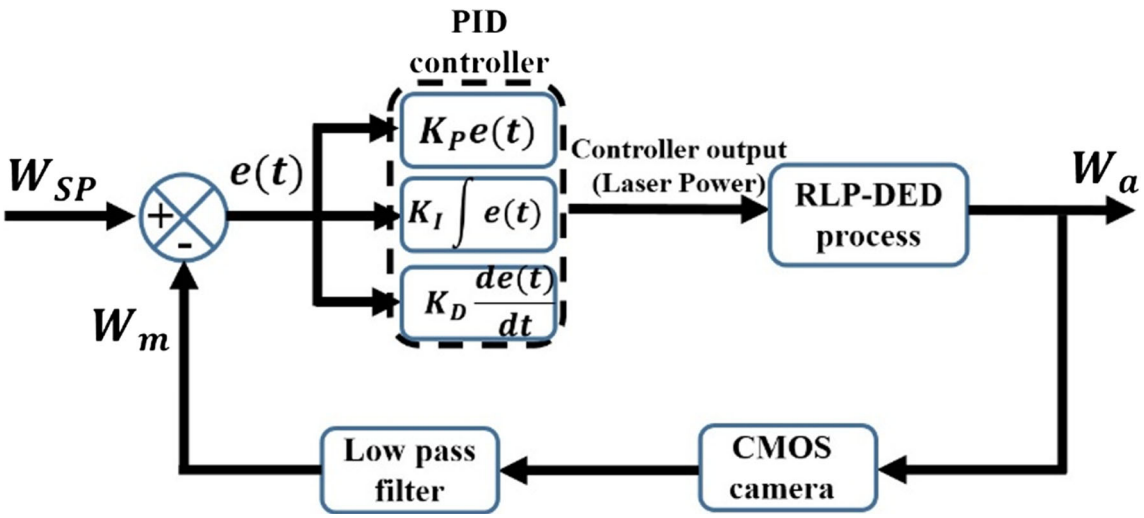

Fig. 5 The block diagram of the closed loop control system used for RLP-DED process

Table 3 Transfer function parameters and controller gains for different layers

Layer no.	t_d (ms)	K	τ (ms)	K_c	T_i (s)
2	250	0.0015	115	1.40	0.15
3	195	0.0024	100	1.41	0.13
4	205	0.0018	120	1.36	0.18
5	180	0.0024	170	1.42	0.2
6	200	0.0021	164	1.53	0.25
7	245	0.0018	190	1.58	0.25
8	260	0.0024	230	1.61	0.38
9	146	0.0027	255	1.65	0.4
10	150	0.0024	250	1.62	0.4

The data from Table 3 reveals that while there was no obvious change in the time delay (t_d) and process gain (K), there existed a gradual increase in the time constant (τ). An increase in the time constant implies that the process became slower as the layer number increased. The faster response of the system in the bottom layers might be attributed to the fast heat sink into the substrate, whereas, moving towards the 9th layer, the heat conduction mode changed from 3D to 2D and resulted in slower dynamic response. However, it was observed that after the 8th layer, the time constant remained almost steady at around 250 ms. This result may be related to the heat saturation; hence, heat exchange reached a quasi-steady status [9]. Moreover, there were no obvious variations in t_d and K beyond the 8th layer up to the last layer of the sample. Therefore, the parameters K_c and T_i were fixed at 1.62 and 0.4, respectively, in the controller for the layers after the 8th. From the control engineering standpoint, an increase in τ moves the closed loop control system in the direction of more stability, allowing a higher proportional gain without the risk of oscillation. This gain is seen from Table 3 where K_c increased from the 2nd to 8th layers. The integral action (T_i) can be looked upon as the impatience level in the controller. As the process became slower in the upper layers, it allowed the controller to become more impatient; thereby, higher integral actions were achieved. In summary, the non-linear relation between the laser power and melt pool width resulted in different controller gains for a thin wall deposition. To verify the performance of the controller, a 160-layer thin wall part was deposited, which will be discussed in this paper.

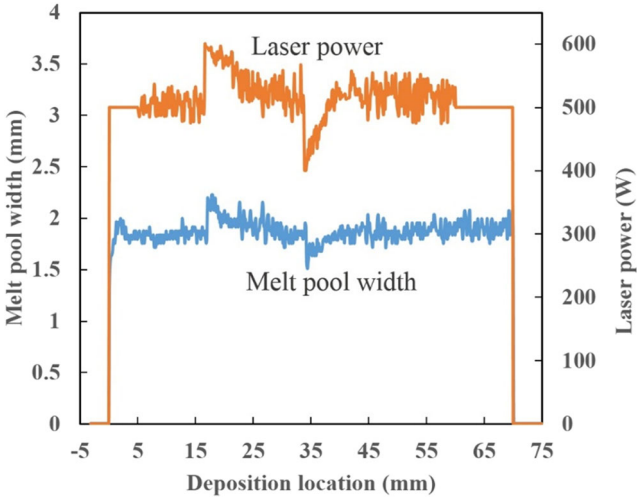

Fig. 6 Response of the closed loop system to disturbances

4 Experimental results and discussion

4.1 Performance verification of controller

Figure 6 depicts the closed loop performance of the controller. Two-step disturbances in the laser power were applied in the closed loop system. One positive step change varied abruptly from 500 to 600 W, and the other negative step change varied from 500 to 400 W. As is observed from Fig. 6, the controller successfully responds to the sudden variations in melt pool width and compensates with a change in the laser power until the melt pool reaches the desired set point.

4.2 Deposition of thin wall structures with and without control

Figure 7 displays the thin wall samples with 160 layers along with their cross sections at the bottom, middle, and top of the depositions. The sample with a constant laser power (600 W) is shown in Fig. 7a. A gradual increase in the melt pool width is clearly seen from bottom towards the top layers. This non-uniform wall thickness was mainly attributed to the change in heat transfer mode. In the first layers, close to substrate, an intense heat sink caused a significant reduction in the melt pool width size. As process continued, the constant laser power led to heat accumulation; thereby, a wider melt pool was achieved progressively.

In current study, all process parameters such as laser power (in the case of sample without control), scanning speed, and powder feed rate are set as fixed values and their effects on the process are not studied. However, the effects of these process parameters on melt pool characteristics (size, temperature, geometry, fluid dynamics) and cooling rate are well-investigated in literature [17, 18]. In general, by increasing the laser power, the melt pool geometrical features (depth, width, length and surface area) and melt pool temperature increase, while by increasing the scanning speed, all those geometrical features and melt pool temperature decrease.

In order to overcome the issue associated with constant laser power in this study, a PI controller with adaptable transfer function as discussed in Sect. 3.3 was utilized. Due to the

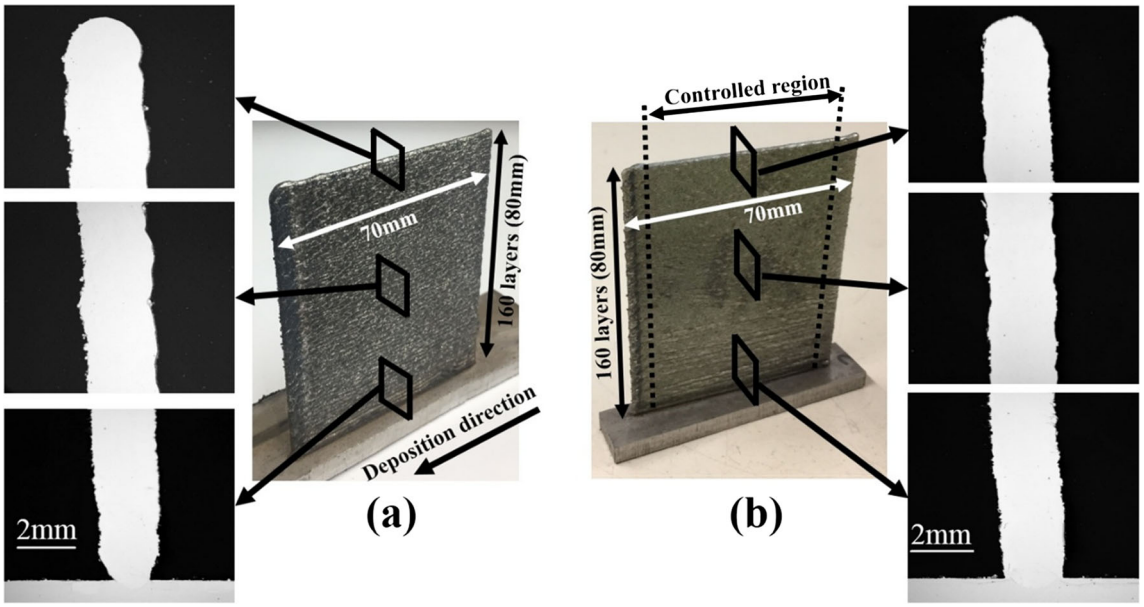

Fig. 7 The deposited samples along with their micrographs. **a** Sample with constant laser power. **b** Sample with controlled laser power

acceleration and deceleration of the robot at the start and end of each bead, larger melt pools were produced in these regions. Therefore, the controller was turned on after 5 mm from the start point and turned off 10 mm before the end of track. Moreover, since the transfer function was not available in the first layer, the controller was turned off, and a constant laser power (750 W) was set for this layer. It should be noted that to avoid very high or very low laser power, a minimum and maximum range was adjusted. The minimum laser power was set at 350 W and the maximum at 700 W. These limit values for the laser power were obtained by trial and error deposition of tracks with laser powers out of the range. In the tracks deposited with less than 350 W laser power, insufficient heat input into the melt pool caused lack-of-fusion defects and delamination between deposition and substrate. Also, in the tracks with laser power higher than 700 W, excessive energy caused the remelting of a large portion of previously deposited layers and consequently an instability led to stop the process. As is seen from Fig. 7b, the cross sections of the buildup have a uniform thickness throughout the entire build.

The result of real-time measurements of the melt pool width for a constant laser power thin wall is displayed in Fig. 8. The significant increase of width in the first several layers and gradual increase in upper layers are also obvious from Fig. 8.

Figure 9 shows the variation of the melt pool width for the controlled thin wall. A constant width was observed from real-time measurements. The corresponding adjusted laser power by the controller is also shown in Fig. 9b. It shows that the laser power gradually decreases from 640 W in the 2nd layer to 510 W in the 160th layer.

4.3 Microstructural analysis

The optical microscope observations revealed no evidence of large porosity, lack of fusion, or cracks. The transverse cross sections of both samples, i.e., the sample with constant laser power and the sample with controlled laser power, were examined at the bottom, middle, and top of the depositions as are seen from Figs. 10 and 11. The morphology mainly consisted of austenitic cells as the primary phase with ferrite at cell

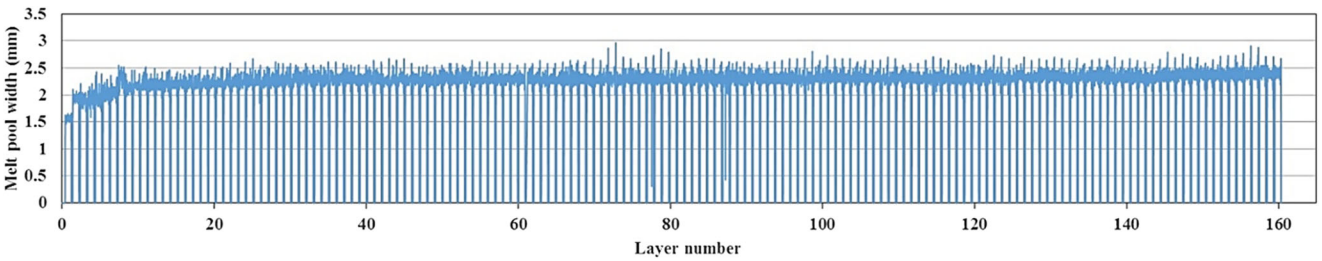

Fig. 8 Melt pool width as a function of layer numbers for the sample with constant laser power

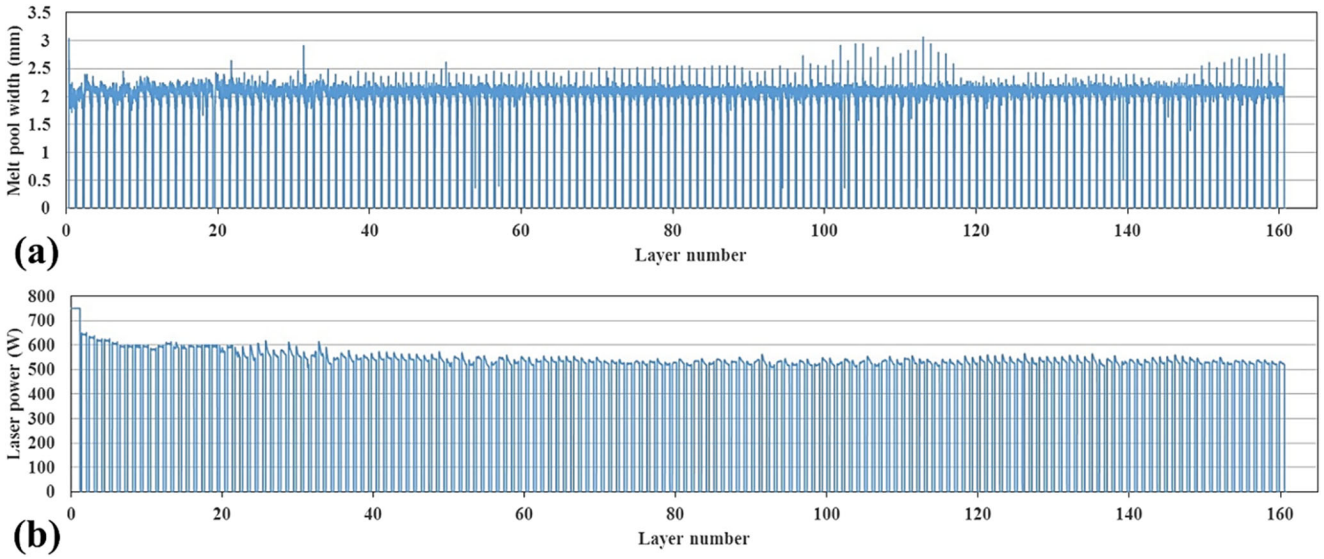

Fig. 9 **a** The variations of melt pool width and **b** laser power for the sample with controlled laser power

boundaries. The microsegregation at grain boundaries during solidification causes the compositional variations [19] and eventually results in producing darker regions that outline the austenite cells after etching, as is seen from Figs. 10 and 11. Figures 10a and 11a illustrate the low magnification of microstructure at the middle of samples. The laser tracks can be clearly observed. The general morphology of the microstructure consisted of a mixture of cellular and columnar dendritic structures. Various portions of cellular, columnar, and dendrite structures with secondary arm spacing were observed at different locations of the cross sections. In the microstructure of the sample with constant laser power, there exists a fine cellular structure in first several layers (Fig. 10b) that gradually change to the combination of columnar and cellular structures in the middle (Fig. 10c). Further, in the top layers, the coarse columnar grains are dominant and even dendrites with secondary arm spacing are visible (Fig. 10d). While the dendritic grain growth is randomly oriented in some areas, a directional solidification is observed in particular regions (Fig. 10a). The directional solidification is a common microstructure orientation for laser-processed parts and is the result of a high solidification rate and temperature gradients [20]. In the case of sample with controlled laser power (Fig. 11b–d), the microstructural observation revealed that the entire structure of sample consisted of only cellular grains, having different cell sizes in different locations of cross sections. This is attributed to the effect of controller on reducing the heat input and thereby producing relatively finer and more homogenous and uniform microstructure.

As shown in Fig. 12, the solidification map could be used to explain the variations in size and morphology of the microstructure. The two most important factors in describing the solidification map are temperature gradient and solidification rate. The temperature gradient, G, is defined as the tangent of the temperature profile of the melt pool with respect to distance. The solidification rate or

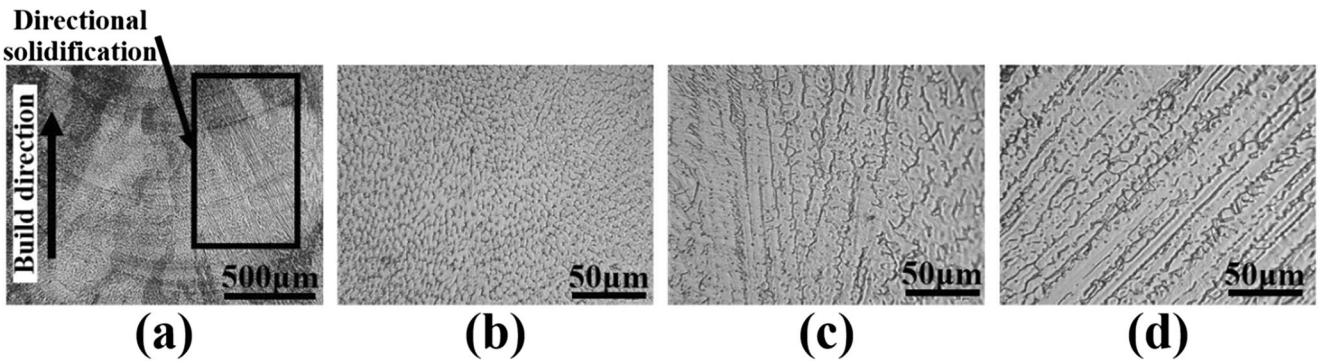

Fig. 10 Microstructure of 316L sample with constant laser power. **a** Low magnification of micrograph at middle of sample. **b** Typical fine cellular structure at bottom layers. **c** Cellular and columnar morphology at middle. **d** Columnar dendritic structure at top layers

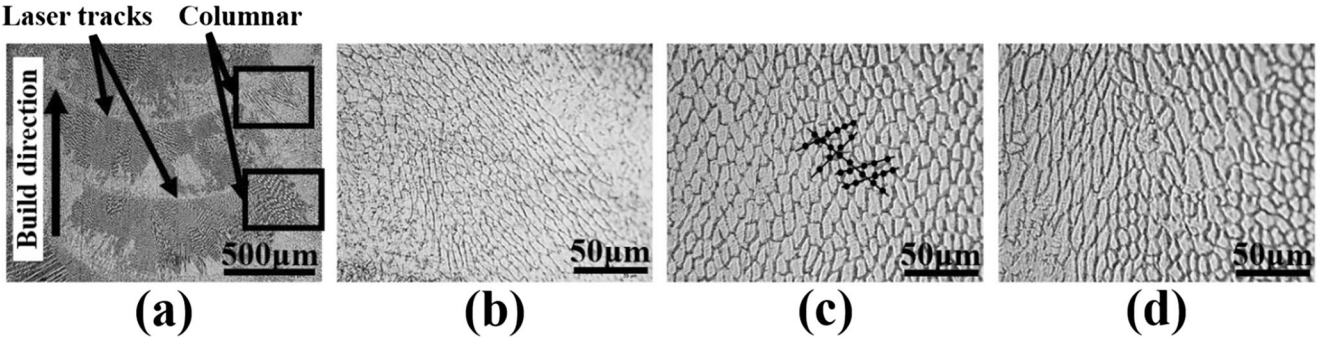

Fig. 11 Microstructure of 316L sample with controlled laser power. **a** Low magnification of micrograph at middle of sample. Cellular structures at **b** bottom layers, **c** middle, and **d** top layers. The method of grain size measurement is shown in **c**

growth rate, R, is the travel velocity of the solid/liquid interface. While the product, GR, which is also defined as the cooling rate, governs the size of the solidification structure, the ratio, G/R, is an important factor in determining the morphology preference of solidification (e.g., planar, cellular, columnar, or equiaxed dendritic) [21].

The temperature of the melt pool progressively increased layer by layer due to the decreased heat conduction through the substrate. Moreover, the temperature gradient reduced in the upper layers because of heat accumulation. Therefore, the ratio, G/R, which defines the stability of solidification front, decreased as new layers were deposited [23]. Eventually, the variations in G/R determined the morphology preference in the final solidification, that is, the transition from cellular in the first several layers to columnar dendritic in the last layers of the sample with constant laser power (Fig. 10). The cooling rate, GR, was also diminished as the layer number increased.

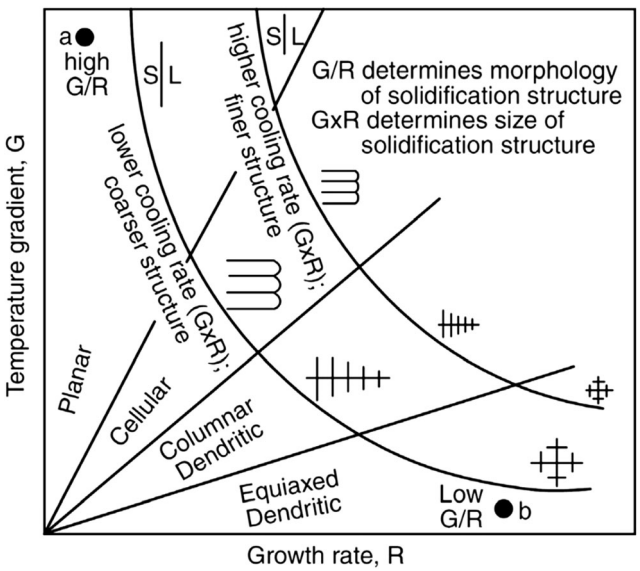

Fig. 12 Solidification map showing the effect of temperature gradient, G, and growth rate, R, on the morphology and size of solidification microstructure [22]

The reduction in cooling rate resulted in enlargement of grains, i.e., the increase in cell size from the bottom towards top layers. Therefore, based on the microstructural observations, it can be concluded that the sample with controlled laser power would have experienced smaller variations in G/R and GR during the solidification.

The grain size was measured across transverse cross sections of both samples, i.e., the sample with constant laser power and the sample with controlled laser power. The measurements were repeated three times in each area in order to increase the accuracy of data. The mean intercept method was utilized to measure the grain size [24]. The average grain size is calculated by dividing the length of set of lines (randomly drawn) by the number of intersected grain boundaries in the optical micrographs. Figure 11c shows the schematic sketch for measuring grain size by the mean intercept method. The result of the grain size measurements is displayed in Fig. 13a. The effect of the closed loop control system is obvious in Fig. 13. Although there was a slight increase in grain size, the sample with controlled laser power generally showed more homogeneous and relatively finer microstructure than the sample with constant laser power. In order to calculate the cooling rate, a well-known empirical equation that relates the cooling rate, $\dot{T}$, and grain size, λ, for 316 stainless steel was used [25].

$$\lambda = 80\dot{T}^{-0.33} \tag{7}$$

Equation (7) could provide an approximation of cooling rates at different locations of buildup. The results are illustrated in Fig. 13b. In the first 20 layers, the error bar shows a larger variation of cooling rates in each layer. As the process continues, more stability in the system leads to small variations as is seen in Fig. 13b.

Figure 13b also demonstrates that the sample with a constant laser power experienced a larger variation in cooling rate across vertical distance as compared to the laser power controlled sample. The result indicated that the closed loop

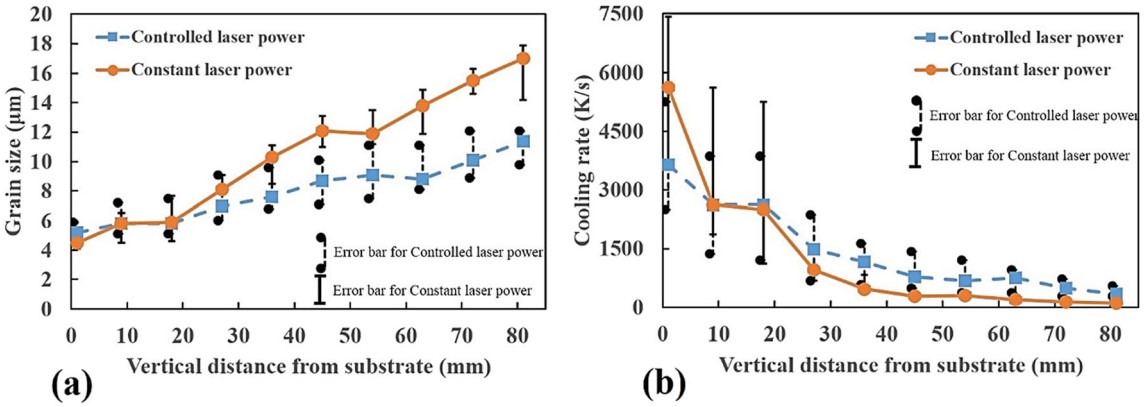

Fig. 13 The variations in **a** grain size and **b** cooling rate as a function of layer number

controller in this study that was designed based on the vision system could be used to control, to some extent, the cooling rate and microstructural properties of the buildups. In a similar study by Hofmeister et al. [26], it was found that in the laser powder deposition process, the cooling rate at the liquid/solid interface had a reverse relation to the square of the melt pool length. Therefore, in a feedback control system, the length of the melt pool can be maintained by online adjustment of laser power, leading to a tailored microstructural property of the buildup. Akbari et al. [27] also used a camera-based monitoring system to measure the melt pool area in the laser wire metal deposition process. They were able to correlate the cooling rate with the melt pool area. They proposed an empirical relation and suggested that the system could be used in the closed loop process in order to adjust the cooling rate in real time.

5 Conclusions

A process monitoring control system based on an infrared image of the melt pool was developed and evaluated by deposition of thin wall samples. The main conclusions from the results are as follows:

- The robotized laser power–directed energy deposition is a non-linear process. Fixed controller gains could not guarantee a good performance of the control system, because the dynamic response between melt pool width and laser power changed during the first 10 layers of deposition.
- An adaptable PI controller that corresponded to the different responses of the system in different layers was developed based on the data from step tests.
- The results of real-time measurement showed that by adjusting the laser power, the controller could successfully ensure a constant size of melt pool width through the entire build.
- Microstructural analysis revealed a small increase in the grain size of the sample with controlled laser power, while in the process without control, there was a larger increase in grain size and in some locations a cellular-to-columnar dendritic transition occurred in the morphology. Also, a lower variation of cooling rate was achieved when the controller was applied in the system.

Acknowledgments The authors express their thanks to Andrew Socha, the research engineer at the Research Center for Advanced Manufacturing for his assistance during the project.

Funding information The authors received financial support from NSF with Grant No. IIP-1539853.

References

1. Williams SW, Martina F, Addison AC, Ding J, Pardal G, Colegrove P (2016) Wire + arc additive manufacturing. Mater Sci Technol 32(7):641–647
2. Uriondo A, Esperon-Miguez M, Perinpanayagam S (2015) The present and future of additive manufacturing in the aerospace sector: a review of important aspects. Proc Inst Mech Eng G J Aerosp Eng 229(11):2132–2147
3. Additive Manufacturing—General Principles—Terminology (2015) ISO/ASTM 52900. International Organization for Standardization, Geneva
4. Fotovvati B, Etesami SA, Asadi E (2019) Process-property-geometry correlations for additively-manufactured Ti–6Al–4V sheets. Mater Sci Eng A 760:431–447
5. Hu D, Kovacevic R (2003) Sensing, modeling and control for laser-based additive manufacturing. Int J Mach Tools Manuf 43(1):51–60
6. Wilson JM, Piya C, Shin YC, Zhao F, Ramani K (2014) Remanufacturing of turbine blades by laser direct deposition with its energy and environmental impact analysis. J Clean Prod 80: 170–178
7. Ding Y, Akbari M, Gao XL, Ai L, Kovacevic R (2018) Use of powder-feed metal additive manufacturing system for fabricating metallic metamaterials. In: Manufacturing techniques for materials: engineering and engineered. CRC Press, pp 51–65
8. Liu W, Wei H, Huang C, Yuan F, Zhang Y (2019) Energy efficiency evaluation of metal laser direct deposition based on process

characteristics and empirical modeling. Int J Adv Manuf Technol 102(1–4):901–913
9. Bi G, Gasser A, Wissenbach K, Drenker A, Poprawe R (2006) Characterization of the process control for the direct laser metallic powder deposition. Surf Coat Technol 201(6):2676–2683
10. Farshidianfar MH, Khajepour A, Gerlich AP (2016) Effect of real-time cooling rate on microstructure in laser additive manufacturing. J Mater Process Technol 231:468–478
11. Ding Y, Warton J, Kovacevic R (2016) Development of sensing and control system for robotized laser-based direct metal addition system. Addit Manuf 10:24–35
12. Hofman JT, Pathiraj B, Van Dijk J, De Lange DF, Meijer J (2012) A camera based feedback control strategy for the laser cladding process. J Mater Process Technol 212(11):2455–2462
13. Heralić A, Christiansson AK, Ottosson M, Lennartson B (2010) Increased stability in laser metal wire deposition through feedback from optical measurements. Opt Lasers Eng 48(4):478–485
14. Kovacevic R, Valant ME (2006) Powder delivery system and method, US7045738B1
15. Mazumder J, Schifferer A, Choi J (1999) Direct materials deposition: designed macro and microstructure. Mater Res Innov 3(3): 118–131
16. Goodwin GC, Graebe SF, Salgado ME (2001) Control system design. Prentice Hall, Upper Saddle River
17. Fotovvati B, Wayne SF, Lewis G, Asadi E (2018) A review on melt-pool characteristics in laser welding of metals. Adv Mater Sci Eng 2018:1–18
18. Liu Z, Li T, Ning F, Cong W, Kim H, Jiang Q, Zhang H (2019) Effects of deposition variables on molten pool temperature during laser engineered net shaping of Inconel 718 superalloy. Int J Adv Manuf Technol 102(1–4):969–976
19. Zheng B, Zhou Y, Smugeresky JE, Schoenung JM, Lavernia EJ (2008) Thermal behavior and microstructure evolution during laser deposition with laser-engineered net shaping: part II. Experimental investigation and discussion. Metall Mater Trans A 39(9):2237–2245
20. Gäumann M, Henry S, Cleton F, Wagniere JD, Kurz W (1999) Epitaxial laser metal forming: analysis of microstructure formation. Mater Sci Eng A 271(1–2):232–241
21. Kurz W, Giovanola B, Trivedi R (1986) Theory of microstructural development during rapid solidification. Acta Metall 34(5):823–830
22. Kou S (2003) Welding metallurgy. John Wiley & Sons
23. Manvatkar V, De A, DebRoy T (2014) Heat transfer and material flow during laser assisted multi-layer additive manufacturing. J Appl Phys 116(12):124905
24. ASTM (2013) E112-13, Standard test methods for determining average grain size. ASTM International, West Conshohocken www.astm.org
25. Elmer JW, Allen SM, Eagar TW (1989) Microstructural development during solidification of stainless steel alloys. Metall Trans A 20(10):2117–2131
26. Hofmeister W, Griffith M (2001) Solidification in direct metal deposition by LENS processing. JOM 53(9):30–34
27. Akbari M, Kovacevic R (2018) An investigation on mechanical and microstructural properties of 316LSi parts fabricated by a robotized laser/wire direct metal deposition system. Addit Manuf 23:487–497